Developmental Cell
Article

Minus-End-Directed Kinesin-14 Motors Align Antiparallel Microtubules to Control Metaphase Spindle Length

Austin J. Hepperla,[1,4] Patrick T. Willey,[1,4] Courtney E. Coombes,[1] Breanna M. Schuster,[1] Maryam Gerami-Nejad,[1] Mark McClellan,[1] Soumya Mukherjee,[1] Janet Fox,[2] Mark Winey,[2] David J. Odde,[3] Eileen O'Toole,[2] and Melissa K. Gardner[1,*]

[1]Department of Genetics, Cell Biology, and Development, University of Minnesota, Minneapolis, MN 55455, USA
[2]MCD Biology, University of Colorado, Boulder, CO 80309, USA
[3]Department of Biomedical Engineering, University of Minnesota, Minneapolis, MN 55455, USA
[4]Co-first author
*Correspondence: klei0091@umn.edu
http://dx.doi.org/10.1016/j.devcel.2014.07.023

SUMMARY

During cell division, a microtubule-based mitotic spindle mediates the faithful segregation of duplicated chromosomes into daughter cells. Proper length control of the metaphase mitotic spindle is critical to this process and is thought to be achieved through a mechanism in which spindle pole separation forces from plus-end-directed motors are balanced by forces from minus-end-directed motors that pull spindle poles together. However, in contrast to this model, metaphase mitotic spindles with inactive kinesin-14 minus-end-directed motors often have shorter spindle lengths, along with poorly aligned spindle microtubules. A mechanistic explanation for this paradox is unknown. Using computational modeling, in vitro reconstitution, live-cell fluorescence microscopy, and electron microscopy, we now find that the budding yeast kinesin-14 molecular motor Kar3-Cik1 can efficiently align spindle microtubules along the spindle axis. This then allows plus-end-directed kinesin-5 motors to efficiently exert the outward microtubule sliding forces needed for proper spindle bipolarity.

INTRODUCTION

During cell division, a microtubule-based mitotic spindle mediates the faithful segregation of duplicated chromosomes into daughter cells. Stable length control of the metaphase spindle is crucial to ensuring the fidelity of chromosome segregation during this process. This is thought to be achieved through a mechanism in which outwardly directed forces from plus-end-directed kinesin-5 molecular motors (which act to push spindle poles apart) are balanced by inwardly directed forces from minus-end motors (which act to pull spindle poles together) (reviewed in Goshima and Scholey, 2010 and Subramanian and Kapoor, 2012). A clear prediction from this model is that metaphase spindles with inactive minus-end-directed kinesin-14 motors should have longer mitotic spindle lengths, due to a reduction in inwardly directed forces. However, the opposite phenotype has frequently been observed (Table 1). For example, knockdown of the human kinesin-14 HSET by RNAi leads to short spindles, even though pole formation remains unaffected (Cai et al., 2009), and fission yeast mitotic spindles are substantially shorter in the absence of the kinesin-14 molecular motor Pkl1 (Troxell et al., 2001). In general, the absence or inactivation of kinesin-14 molecular motors has been correlated with disorganized and often shorter mitotic spindles across a wide range of organisms (Table 1). A mechanistic explanation for this phenomenon is unknown.

To maintain a stable metaphase spindle length, plus-end-directed kinesin-5 motors are responsible for sliding oppositely oriented microtubules apart to stably separate the spindle poles or centrosomes (Enos and Morris, 1990; Kashina et al., 1996; Sawin et al., 1992). However, this action requires the prior establishment of a functional spindle "midzone" that is made up of microtubules that are closely aligned along the spindle axis, so that the kinesin-5 motors can properly crosslink and slide antiparallel spindle microtubules. In budding yeast, the minus-end-directed kinesin-14 Kar3 is one of only two motors that are required for proper spindle assembly (Cottingham et al., 1999), which hints that kinesin-14 motor proteins could perhaps have a role in the assembly and maintenance of a functional spindle midzone and thus act to facilitate proper force generation by kinesin-5 molecular motors.

We now find that the yeast kinesin-14 molecular motor Kar3-Cik1 efficiently organizes microtubules into a functional spindle midzone by virtue of the motor's minus-end-directed motility. This enables plus-end-directed kinesin-5 motors to exert the outward microtubule sliding forces needed for spindle bipolarity. Here, spindle microtubule minus ends that are anchored at the poles act as spatial positioning guides that are used by the kinesin-14 Kar3-Cik1 motors to pivot microtubules into alignment with the central spindle axis. Our results demonstrate how simple rules for minus-end motor directionality and the polarity of microtubule attachment could lead to a functional spindle midzone inside of cells.

RESULTS

Kar3-Cik1 Is the Predominant Yeast Kinesin-14 Heterodimer that Regulates Spindle Length and Morphology

Inside of cells, the yeast kinesin-14 molecular motor Kar3 does not act as a functional monomer or homodimer, but rather

Table 1. Mitotic Spindle Length and Kinesin-14 Molecular Motors

Organism (Kinesin-14 Protein)	Effect on Spindle Length	Reference
H. sapiens (HeLa cells: HSET)	spindles ~20% shorter in HSET RNAi	Cai et al., 2009
S. pombe (Pkl1, Klp2)	spindles are ~11% shorter in *pkl1Δ* spindles are ~5% longer in klp2Δ	Troxell et al., 2001
D. melanogaster (S2 cells: Ncd)	*overexpression* of Ncd caused a dose-dependent elongation of the metaphase spindle Ncd RNAi caused splaying of microtubules and slight increase in spindle length	Goshima et al., 2005
S. cerevisiae (Kar3)	short mitotic spindles and disrupted spindle structure in *kar3Δ*	Meluh and Rose, 1990; Saunders et al., 1997a
X. laevis (XCTK2)	a 4-fold increase in monopolar spindles and unstable spindle length in the presence of anti-XCTK2 antibodies	Walczak et al., 1998
A. thaliana (ATK5)	spindle width at midzone significantly larger in *atk5-1* compared with WT cells	Ambrose and Cyr, 2007
C. albicans (Kar3)	well-defined mitotic spindles missing in $kar3^{-/-}$	Sherwood and Bennett, 2008
D. melanogaster (embryos: Ncd)	overall rate and extent of spindle pole separation is greater, and there is poor spindle structure and spindle microtubule alignment in *absence* of Ncd	Sharp et al., 2000

This table summarizes previously published literature that describes the effect of kinesin-14 disruptions on mitotic spindle phenotypes.

selectively heterodimerizes with either of two different accessory proteins, Cik1 or Vik1 (Barrett et al., 2000; Gardner et al., 2008b; Manning et al., 1999; Page and Snyder, 1992) (Figure 1A). Importantly, Cik1 and Vik1 both associate with Kar3 through their coiled-coil domains, which allows for a second microtubule-binding site at the tail in addition to Kar3 motor-head binding (Figure 1A). Specifically, we note that the *cik1Δ* mutant disrupts the microtubule crosslinking ability of the Kar3-Cik1 motor: previously published in vivo studies demonstrated that interaction of Cik1 with Kar3 was required for association of the nonmotor domain of Kar3 to microtubules, while motor domain binding of Kar3 did not require Cik1 (Page et al., 1994; Page and Snyder, 1992). Therefore, Kar3 does not crosslink microtubules in the absence of the accessory protein Cik1, even though microtubule binding of the Kar3 motor domain would still occur (Allingham et al., 2007; Barrett et al., 2000; Manning et al., 1999; Meluh and Rose, 1990).

Previous data suggest that Kar3-Cik1 has a substantially more important role in maintaining the structural stability of the yeast anaphase spindle than does Kar3-Vik1 (Gardner et al., 2008b). However, the differential effects of Kar3-Cik1 and Kar3-Vik1 on metaphase spindle structure have not been examined. Therefore, budding yeast strains with labeled microtubules (Tub1-GFP) and spindle poles (Spc110-mCherry) were used to examine wild-type (WT), *cik1Δ*, *vik1Δ*, and *kar3Δ* metaphase spindles. Here, total internal reflection fluorescence (TIRF) microscopy of coverslip-adhered live yeast cells was used to observe spindle length and general spindle structure (Figure 1B). Qualitatively, it was found that WT metaphase spindles appeared longer and had tightly aligned microtubules (Figure 1B, top), while spindles in *vik1Δ* and especially in *cik1Δ* were shorter and appeared to have frequent "stray" microtubules emanating from spindle poles (Figure 1B, center). Similarly, *kar3Δ* spindles, which are expected to show characteristics of both *cik1Δ* and *vik1Δ* spindles, also appeared shorter and less tightly aligned than the WT metaphase spindles (Figure 1B).

To quantify this observation, metaphase spindle length and width were assessed in each case. First, spindle length was measured as the distance between the red Spc110-mCherry pole markers along the spindle axis (Figure 1C). Here, we found that while metaphase spindle lengths were significantly shorter in both *cik1Δ* and *vik1Δ* spindles compared to WT spindles (Figure 1C; $p << 0.0001$, t test: both comparisons), the *cik1Δ* spindles were, on average, shorter than the *vik1Δ* spindles ($p << 0.0001$, t test: *cik1Δ* versus *vik1Δ*) (Roof et al., 1991, 1992; Saunders et al., 1997b; Saunders and Hoyt, 1992). Second, the approximate metaphase spindle width was quantified by fitting a Gaussian distribution to the integrated tubulin-associated fluorescence above and below the spindle axis (Figure 1D). While this method is inherently noisy, there was a general trend toward wider spindles in the kinesin-14 deletion mutants, and especially for the *cik1Δ* spindles (Figure 1D). Thus, quantitative analysis of microtubule-associated spindle fluorescence inside of cells suggests that interpolar microtubules in metaphase spindles are misaligned in the kinesin-14 deletion mutants, and particularly in the absence of Cik1 compared to Vik1 (Figure S1 available online).

Kar3-Cik1 Targets Spindle Microtubules during Metaphase while Kar3-Vik1 Is Targeted to Poles

Consistent with the finding that Kar3 selectively heterodimerizes with either Cik1 or Vik1 (Barrett et al., 2000; Gardner et al., 2008b; Manning et al., 1999), previous in vivo analysis in yeast anaphase spindles demonstrated that Kar3-GFP was localized both at the spindle poles and in punctate spots within the anaphase spindle and that the Kar3-Cik1 complex was primarily responsible for the Kar3-GFP signal within the spindle. In contrast, Kar3-Vik1 was exclusively located near to the spindle poles (Gardner et al., 2008b). Thus, we performed a similar analysis to determine how the accessory proteins Cik1 and Vik1 apportion Kar3-GFP protein on the metaphase spindle. We found that Kar3-GFP is distributed both at the spindle poles,

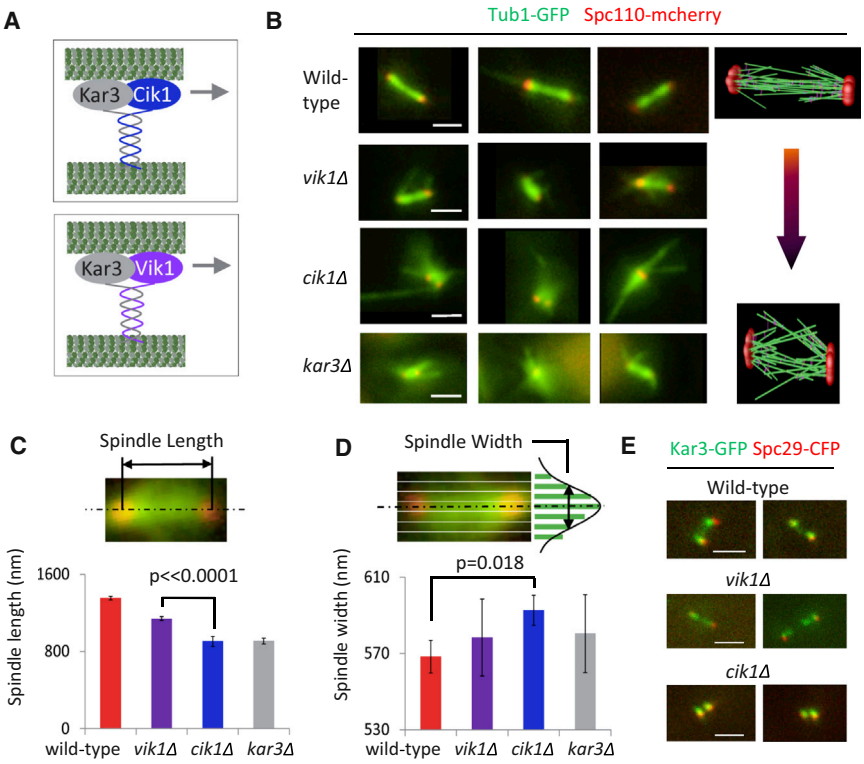

Figure 1. Kar3-Cik1 Molecular Motors Contribute to Proper Metaphase Spindle Length

(A) Kar3 associates with either of two accessory proteins, Vik1 or Cik1, inside of cells.

(B) TIRF microscopy experiments in live cells (scale bar, 1,000 nm).

(C) Quantitative analyses of TIRF microscopy experiments (WT, n = 392; *cik1Δ*, n = 219; *vik1Δ*, n = 209; *kar3Δ*, n = 195; error bars show SEM).

(D) TIRF microscopy experiments demonstrate wider spindles in *cik1Δ* and *vik1Δ* experiments (error bars show SEM).

(E) Localization studies using fluorescence microscopy (scale bar, 500 nm).

and, to a lesser extent, within the metaphase spindle itself (Figure 1E, top). However, in *vik1Δ* spindles, the Kar3-GFP protein within the metaphase spindle appears to be increased relative to the poles, suggesting that Cik1 mediates localization of Kar3 to spindle microtubules (Figure 1E, middle). Conversely, Kar3-GFP is strongly localized to the spindle poles in *cik1Δ* spindles, suggesting that Vik1 mediates localization of Kar3 to the spindle poles rather than to the spindle microtubules (Figure 1E, bottom). Thus, we conclude that the accessory protein Cik1 localizes the Kar3-Cik1 motor to spindle microtubules, and, together with the results that metaphase spindle lengths were significantly shorter in *cik1Δ* spindles compared to *vik1Δ* spindles, we hypothesize that the heterodimeric kinesin-14 molecular motor Kar3-Cik1 may act on spindle microtubules to control metaphase mitotic spindle length. Therefore, we focused the remainder of the investigation exclusively on Kar3-Cik1 and its interactions with spindle microtubules during metaphase.

Metaphase Spindles in *cik1Δ* Mutants Have Improper Microtubule Alignment

Quantitative analysis of microtubule-associated spindle fluorescence suggests that interpolar microtubules were misaligned in metaphase *cik1Δ* spindles (Figure 1D). However, an alternative explanation for the fluorescence imaging results is that *cik1Δ* spindles nucleate additional cytoplasmic or spindle microtubules, as has been previously reported (Huyett et al., 1998; Saunders et al., 1997a). To distinguish between these possibilities, we reconstructed WT and *cik1Δ* yeast metaphase spindles using electron tomography (Figure 2A; Movie S1) and found that the interpolar microtubules were indeed severely misaligned in the shorter *cik1Δ* spindles, leading to a poorly aligned spindle structure (Figure 2A). However, the total number of microtubules attached to the spindle poles (N_{MT}) was similar between WT and *cik1Δ* spindles (Figure S2; $n_{MT,WT}$ = 40 ± 2, $n_{MT,cik1\Delta}$ = 41 ± 1 [mean ± SD]; p = 0.27, t test).

To quantify spindle microtubule alignment in the tomographic models, an analysis was performed that identified those microtubules that were closely spaced and aligned with other microtubules over a substantial distance: "core microtubules" were defined as those that were separated from other microtubules by 45 nm or less over a distance of 300 nm or greater. We found that the *cik1Δ* metaphase spindles in the tomographic reconstructions had more variability in core microtubule numbers than in the WT cells (Figure 2B, left; p = 0.03, f test), and, importantly, that the *cik1Δ* cells with decreased core microtubule numbers tended to also have shorter spindles lengths (Figure 2B, right). Thus, we conclude that (1) the minus-end-directed kinesin-14 motor protein Kar3-Cik1 improves the efficiency of aligning interpolar microtubules in the yeast metaphase spindle and (2) properly aligned spindle microtubules are correlated with longer spindle lengths.

In the electron microscopy (EM) tomographic reconstructions, there were occasional stray spindle microtubules that grew well past the opposite spindle pole body (Figure S2A). Thus, to determine whether overall microtubule length regulation was altered in the *cik1Δ* mutant cells, we measured the length distribution of astral microtubules during mitosis in WT and mutant cells. Here, astral microtubule lengths were similar between WT and *cik1Δ* cells (Figure S1C; p = 0.55, t test). Therefore, we conclude that poorly aligned interpolar microtubules grow beyond the opposite spindle pole in *cik1Δ* spindles as a consequence of their poor alignment along the spindle axis.

Disrupted Spindle Structures in *cik1Δ* Spindles Are Correlated with Reduced Spindle Binding of the Outward-Force-Generating Molecular Motor Cin8

The kinesin-5 molecular motor Cin8 is expected to be the major outward-force-generating spindle motor in budding yeast. This is based in part on previous work that showed that spindle lengths were shorter in *cin8Δ* spindles and longer with Cin8

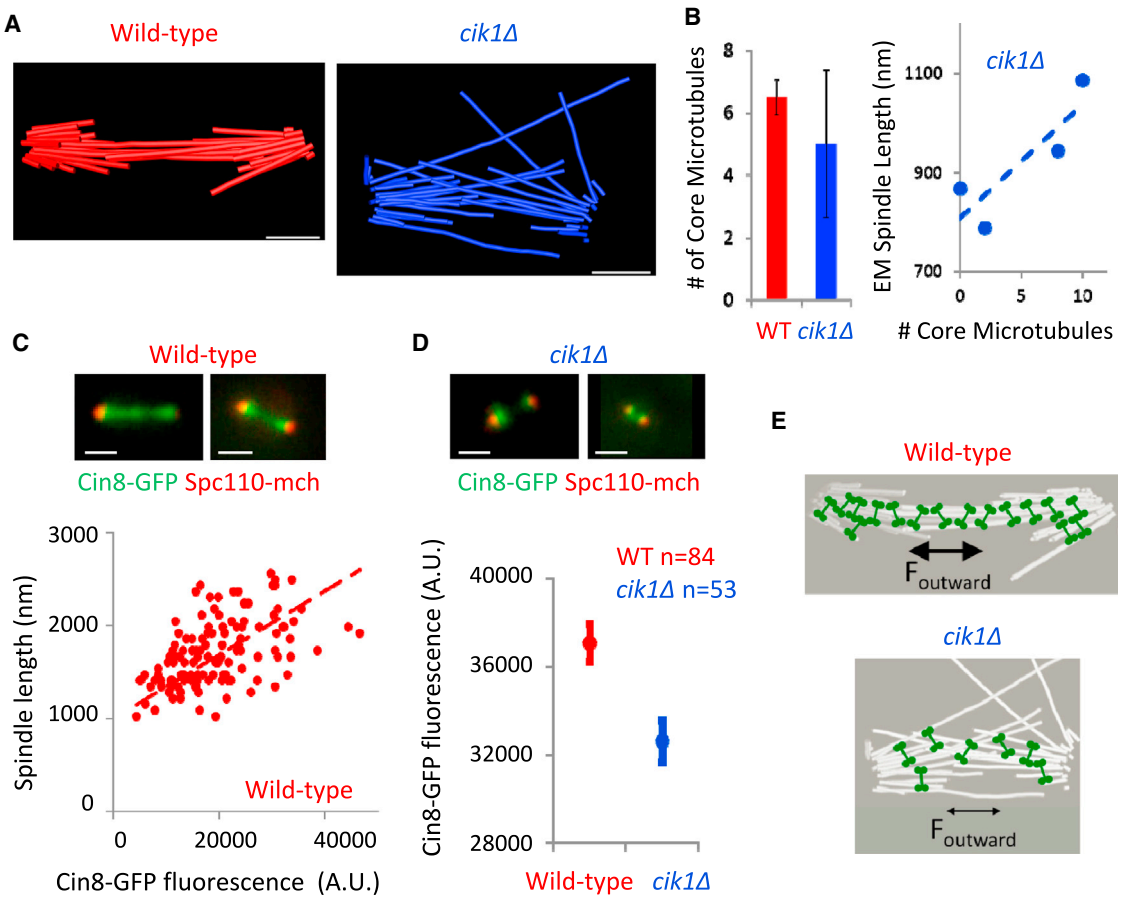

Figure 2. Poor Interpolar Microtubule Alignment in *cik1Δ* Spindles Leads to Shorter Spindle Lengths

(A) Electron tomography experiments in WT (1,128 nm) and *cik1Δ* (868 nm) spindles.

(B) Core microtubule number in *cik1Δ* (n = 4) compared to WT spindles (n = 6). Reduced core microtubule number was associated with shorter *cik1Δ* spindles (right).

(C) Spindle length is positively correlated with integrated Cin8-GFP fluorescence in WT spindles (p_{zero_slope} << 0.0001, red).

(D) Cin8-GFP localization and attachment appears disrupted in *cik1Δ* metaphase spindles (top: scale bar, 500 nm; bottom: p = 0.0008).

(E) Schematic showing that the kinesin-5 molecular motor Cin8 is not able to properly crosslink unaligned midzone microtubules.

overexpression (Gardner et al., 2008a; Hildebrandt and Hoyt, 2000; Saunders and Hoyt, 1992). Thus, because metaphase spindles are shorter in *cik1Δ* cells, it may be that improper spindle microtubule alignment in *cik1Δ* disrupts proper Cin8 targeting and crosslinking. Here, Cin8, which is unable to crosslink widely spaced interpolar microtubules, may have an increased off-rate, leading to reduced Cin8 targeting in *cik1Δ* spindles.

Thus, we reasoned that reduced Cin8-GFP fluorescence intensity on the spindle may reflect improper Cin8 targeting and therefore be correlated with shorter mitotic spindle lengths. To test this idea, we performed the following proof-of-principle experiments. (1) The Cin8-GFP expression level was gradually increased under a *GAL1* promoter, and spindle length was measured as a function of increasing spindle-bound Cin8-GFP fluorescence (Figure S1). These experiments demonstrated that increased total Cin8-GFP signal was indeed associated with longer spindle lengths, consistent with the hypothesis that an increase in outward-force-generating Cin8 motor binding to the spindle leads to longer spindle lengths (Figure S1). (2) Metaphase spindles labeled with Cin8-GFP and Spc110-mCherry spindle pole markers in live cells were analyzed by simultaneously measuring both spindle length and total Cin8-GFP fluorescence for each spindle. Then, the WT spindle length was plotted against total Cin8-GFP fluorescence for each spindle (Figure 2C). There was a clear positive correlation, such that decreased Cin8-GFP fluorescence was correlated with the shorter spindles (p << 0.0001, linear regression), consistent with the hypothesis that a decrease in outward-force-generating Cin8 motor binding to the spindle leads to shorter spindle lengths (Figure 2C). We conclude that total spindle-bound Cin8-GFP fluorescence provides a readout for spindle microtubule crosslinking by Cin8 and that reduced Cin8-GFP fluorescence on the spindle leads to shorter spindle lengths.

To test whether reduced Cin8 binding in *cik1Δ* spindles may lead to their shorter spindle lengths, the total Cin8-GFP fluorescence was analyzed in *cik1Δ* spindles for comparison to WT cells. The average Cin8-GFP fluorescence was reduced in *cik1Δ* compared to WT spindles (p = 0.0007, t test; Figure 2D).

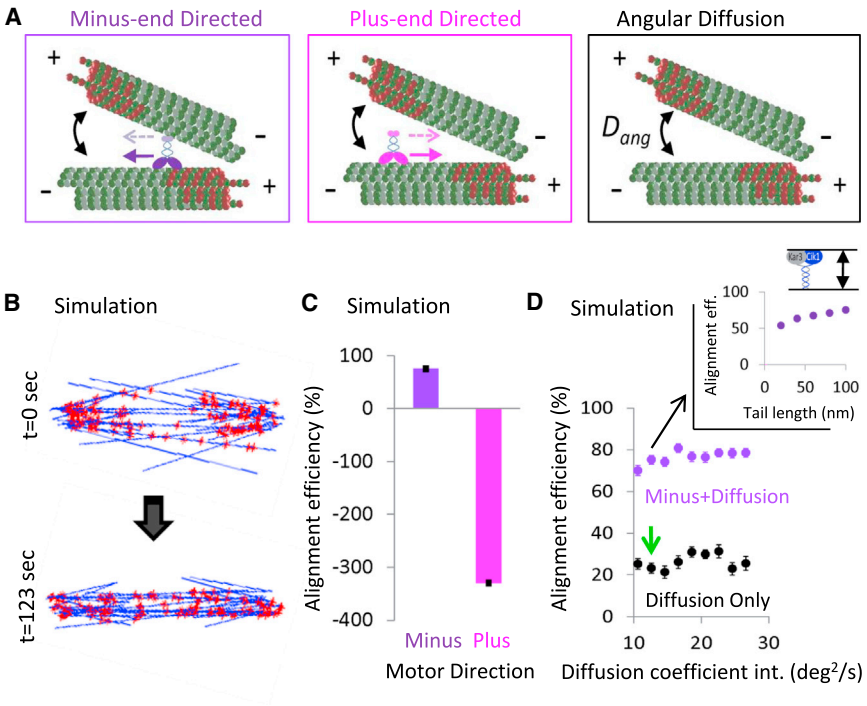

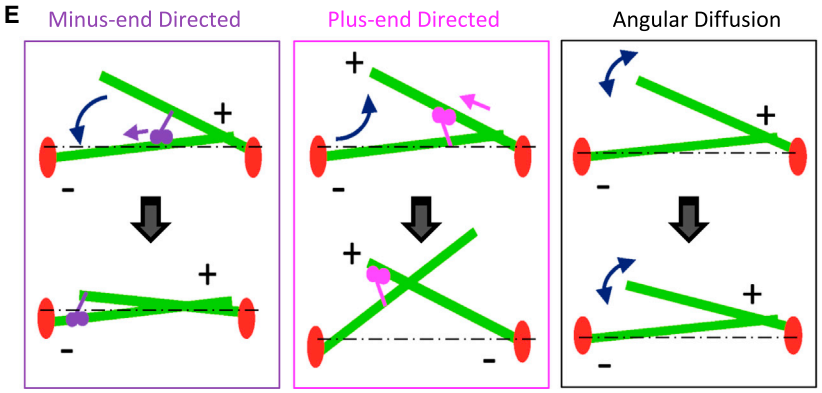

Figure 3. Computational Simulations Predict that Minus-End-Directed Crosslinking Motors Efficiently Align Midzone Microtubules while Plus-End-Directed Motors and Angular Diffusion Do Not

(A) Models for molecular motor-based "zippering" of microtubules to form a mitotic spindle midzone.

(B) Typical simulation starting conditions (top) and potential ending condition (bottom) (blue: microtubules; red: motors).

(C and D) Simulations predict that minus-end-directed motors are more efficient at midzone microtubule alignment than are plus-end-directed motors (C) and passive angular diffusion (D; Movie S2). Green arrow indicates experimentally measured diffusion coefficient intercept (Kalinina et al., 2013) (Figure S3). Inset: alignment efficiency depends weakly on minus-end-directed motor tail length in the simulation.

(E) Simulated minus-end motors promote proper midzone microtubule alignment because they tend to pivot splayed microtubules toward the spindle poles (left). In contrast, plus-end motors tend to pivot spindle microtubules away from the midzone (center), and passive angular diffusion has no positional bias and is thus less efficient at pivoting simulated microtubules into alignment along the spindle axis.

We conclude that disrupted interpolar microtubule alignment in *cik1Δ* spindles (Figures 2A and 2B) leads to reduced binding of outward-force-generating Cin8 molecular motors (Figure 2D), which in turn leads to reduced spindle lengths (Figure 2E).

Simulations Predict that a Minus-End-Directed Crosslinking Molecular Motor Can Efficiently Align Microtubules along the Spindle Axis

Based on our experimental results, poor efficiency in properly aligning interpolar microtubules likely leads to short, unstable mitotic spindles in *cik1Δ* cells, which could have serious consequences for the fidelity of chromosome segregation during mitosis (Kwon et al., 2008; Yuen et al., 2007). Therefore, we used computational simulations to investigate potential mechanisms for how motors could properly align microtubules along the spindle axis during metaphase.

The simulations were used to compare three distinct mechanisms for how microtubules could be properly aligned along the spindle axis: (1) minus-end-directed motors with a second microtubule-binding site on the tail could act as "motile crosslinkers" to pivot microtubules into alignment (Figure 3A, left) (Furuta and Toyoshima, 2008; Shimizu et al., 1995); (2) plus-end-directed motors with a second microtubule-binding site on the tail could similarly pivot microtubules (Figure 3A, center); and (3) angular diffusion could allow interpolar microtubules to passively pivot into alignment (Kalinina et al., 2013). For the minus- and plus-end-directed motor simulations, kinesin motor proteins acted as "motile crosslinkers," such that the walking motor-head bound to one microtubule, and then the tail bound to a separate microtubule. In these simulations, it was assumed that the motor tail would remain bound to a crosslinking microtubule as it trailed the motor-head, i.e., the tail was pulled along on its respective microtubule by the walking motor-head that was attached to its own microtubule (Figure 1A). These simulated motor proteins could be minus-end directed (Figure 3A, left) or plus-end directed (Figure 3A, center) and could potentially pivot spindle microtubules into alignment with the central spindle axis (see Supplemental Experimental Procedures for details and assumptions). The idea that a motile crosslinking motor could align microtubules has been previously demonstrated in vitro using purified kinesin-14 proteins from other organisms, and so represents a reasonable potential mechanism for spindle microtubule alignment (Ghosh et al., 2013; Portran et al., 2013). Alternatively, angular diffusion could allow spindle microtubules to passively pivot into alignment at the midzone (Figure 3A, right) (Kalinina et al., 2013). Note that

in all cases (either with active motors or with passive angular diffusion), it was assumed that once a microtubule plus end was within proximity of the spindle axis (i.e., so that the spindle microtubule was nearly parallel to the spindle axis), other crosslinking proteins would "capture" the microtubule and would thus hold the microtubule in place along the spindle axis for the remainder of the simulation (Schuyler et al., 2003).

To run the simulations, microtubule minus ends were randomly assigned to positions inside of 250-nm-diameter spindle poles, as in previous budding yeast simulations (Gardner et al., 2005). Then, the spindle microtubule plus ends were allowed to "splay" out away from the spindle poles at random 3D angles (t = 0, 0°–30°; Figure 3B, top). This type of configuration would be characteristic of a mitotic spindle with a poorly formed spindle midzone, as was observed in *cik1Δ* spindles (Figure 2A), or which could be present during early spindle formation (O'Toole et al., 1999; Winey et al., 1995). At the simulation completion ($t_{duration}$ = 15 min), we asked whether the simulated molecular motors had "rescued" the splayed phenotype by pivoting microtubules into parallel 3D alignment along the spindle axis (Figure 3B, bottom). Here, an "alignment efficiency" was calculated to provide a quantitative output for rescue success in each case, as follows:

$$eff = 100\left[\frac{\sum angles_{start} - \sum angles_{end}}{\sum angles_{start}}\right]. \quad (1)$$

Here, *eff* is efficiency of microtubule alignment along the spindle axis (%), and $\Sigma angles_{start}$ and $\Sigma angles_{end}$ represent the sum of the absolute values of all 3D angles (θ and φ) for all interpolar microtubules at the start and end of the simulation, respectively, such that $\theta = \varphi = 0°$ represented perfect alignment along the spindle axis for a given spindle microtubule.

We first used the stochastic simulations to compare the ability of the minus-end-directed and plus-end-directed motile crosslinking motors to efficiently align spindle microtubules along the spindle axis. Importantly, while minus-end-directed motors aligned spindle microtubules along the spindle axis with ~75% efficiency over 15 min of simulation time, the corresponding efficiency for plus-end-directed crosslinking motors was negative, suggesting that plus-end-directed motile crosslinkers with a single motor-head could act to misalign antiparallel spindle microtubules, splaying them away from the spindle centerline (Figure 3C; this would not apply to kinesin-5 motors with two motor-heads, as these motors stall on antiparallel microtubules [Kapitein et al., 2005]). Thus, while splayed spindle microtubules were routinely pivoted into 3D alignment with the spindle axis in the minus-end-directed motor simulation (Figure 3B; Movie S2), plus-end-directed motors had the opposite effect: spindle microtubules were, on average, splayed away from alignment with the spindle axis (Figure 3C; Movie S2).

We then used the simulation to predict the relative efficiency of minus-end-directed motors compared to passive angular diffusion in aligning spindle microtubules along the central spindle axis. Passive angular diffusion of interpolar microtubules was included in all simulations, regardless of the presence or absence of active motors, using an empirical fit to previously published microtubule length-dependent angular diffusion coefficients in fission yeast (Kalinina et al., 2013) (Figure S3). However, passive angular diffusion by itself was not sufficient to efficiently align microtubules along the spindle axis in simulation, regardless of the angular diffusion coefficient value tested (Figure 3D, green arrow represents published measurement [Kalinina et al., 2013]).

To ensure that the alignment efficiency result for minus-end-directed motors was robust over a range of tail crosslink lengths, we evaluated the simulated alignment efficiency for a range of motor tail lengths (Figure 3D, inset). Alignment efficiency dropped as a function of decreased motor tail length, but only moderately: there was a 16% drop in simulated efficiency from a 100 nm tail length down to a 40 nm tail length (Figure 3D, inset). Thus, over a range of reasonable tail lengths, simulations predict that minus-end-directed motile crosslinking motors are uniquely able to efficiently align microtubules along the spindle axis to build a functional midzone in yeast metaphase spindles.

Careful examination of spindle simulation movies suggested that the difference in alignment efficiency between plus-end-directed and minus-end-directed motors relied primarily on the localization of microtubule minus ends at the spindle poles: in walking toward the microtubule minus ends at the poles, the crosslinking molecular motors tended to swivel the plus ends of microtubules attached to the opposite pole toward the spindle axis, in line with the two spindle poles (Movie S2; Figure 3E, left, black dashed line shows spindle axis). In contrast, motile crosslinking plus-end-directed motors swiveled microtubules toward the splayed microtubule plus ends and thus tended to splay the microtubule plus ends away from the spindle axis (Movie S2; Figure 3E, center). While the passive angular diffusion simulations did not adversely affect microtubule alignment at the spindle equator, lack of a strong bias toward the spindle centerline decreased the efficiency of the alignment process, such that over a normal metaphase timescale, alignment efficiency remained low (~20%; Movie S2; Figure 3E, right). Thus, the simulations predicted that molecular motors that walk toward spindle poles (i.e., minus-end-directed motors) could align microtubules along the spindle axis.

In Vitro Experiments Demonstrate that Full-Length Kar3-Cik1 Is Minus-End-Directed and Can Crosslink Microtubules

Our in vivo data demonstrated that, on average, spindle microtubules were poorly aligned in *cik1Δ* metaphase spindles, leading to a dysfunctional spindle midzone and shorter spindle lengths. In addition, simulations that predicted a mechanism for spindle microtubule alignment by Kar3-Cik1 required that (1) the full-length motor was minus-end directed and (2) the motor could crosslink and align microtubules. While truncated Kar3-Cik1 has been previously shown to move toward the minus ends of microtubules (Endow et al., 1994; Meluh and Rose, 1990; Middleton and Carbon, 1994; Page et al., 1994), and the heterodimer has been predicted to crosslink microtubules (Barrett et al., 2000), the in vitro behavior of the full-length Kar3-Cik1 complex has not yet been described. Therefore, full-length Kar3-GFP/Cik1-glutathione S-transferase (GST) was purified from budding yeast cells (see Experimental Procedures and Figure S4), and its interaction with rhodamine-labeled guanosine-5′-[(α,β)-methyleno]triphosphate (GMPCPP)-stabilized microtubules was observed in vitro using TIRF microscopy (Figure 4A). We found that the full-length Kar3-Cik1 motor moved quickly and

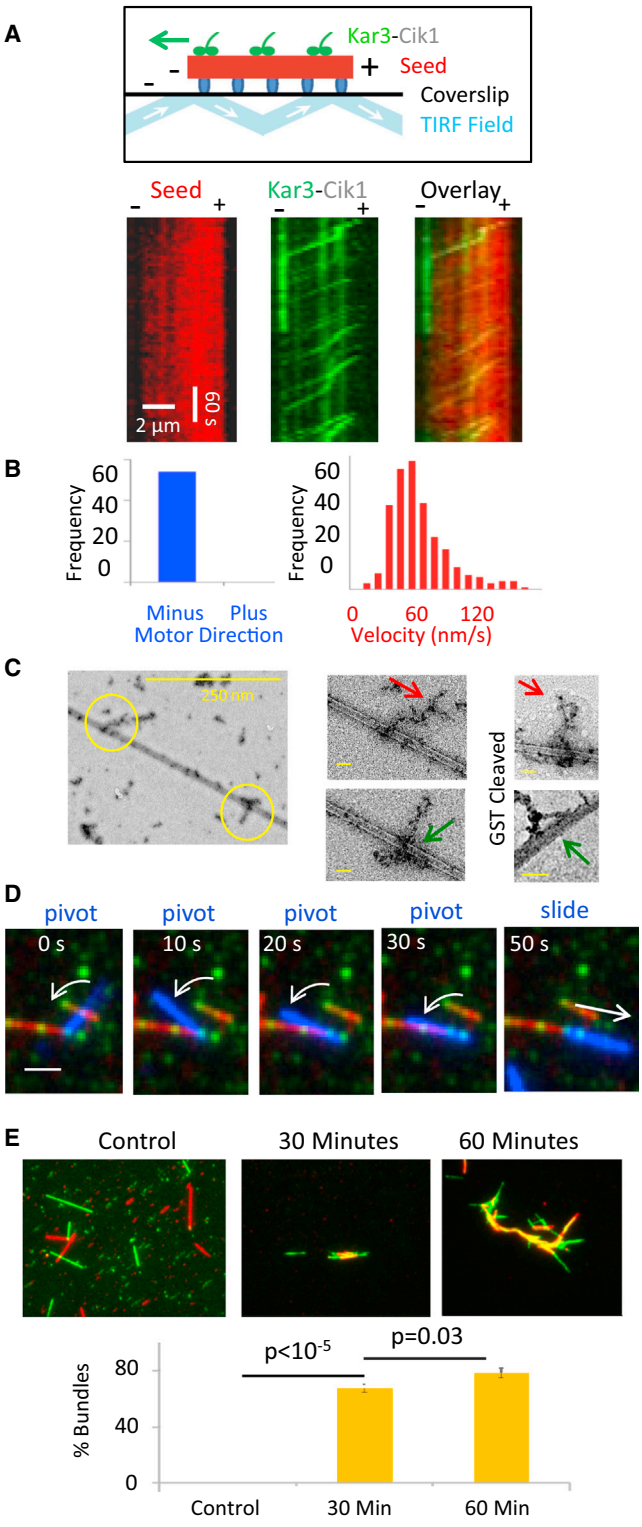

Figure 4. In Vitro Experiments Demonstrate that Full-Length Kar3-Cik1 Is a Processive Minus-End-Directed Molecular Motor that Crosslinks Microtubules

(A) TIRF microscopy assays demonstrated that purified Kar3-GFP/Cik1-GST moves in a processive minus-end-directed manner along a microtubule (dim, minus end; bright, plus-end) (Movie S3).

processively in a minus-end-directed manner along the microtubules: using polarity-marked microtubules, all of the observable motor movements were toward the microtubule minus ends (Movie S3; Figure 4B), regardless of salt concentration tested (Figure S4), and also whether or not the GST tag was cleaved from Cik1 (Figure S4). The mean ± SEM motor velocity over all salt concentrations was 45 ± 2.5 nm/s (Figure S4), which is similar to published values for the kinesin-8 motor Kip3, albeit in the opposite direction (Kip3 velocity ~50 nm/s) (Varga et al., 2006).

To determine whether the range of motor tail lengths was consistent with our simulations, we performed room-temperature negative staining and transmission electron microscopy (TEM) of the microtubule-bound Kar3-Cik1 motor. Here, Kar3-Cik1 motors attached to microtubules appeared to be consistent with single molecules (Figure 4C, left, yellow circles). We speculate that "tail"-attached motors display the motor-head away from the microtubule (Figure 4C, right top, red arrows), and "head"-attached motors display the motor-head attachment on the microtubule (Figure 4C, right bottom, green arrows). We found that the motor tail was significantly longer than the 25 nm microtubule diameter, with a length estimate from our TEM images of 60–100 nm.

In addition to being minus-end directed, the second major assumption in our model for how kinesin-14 molecular motors could effectively align the microtubule-based spindle midzone was in their ability to crosslink microtubules. Therefore, this assumption was also tested using the in vitro assay. Here, rhodamine-labeled GMPCPP microtubules were attached to coverslips using anti-rhodamine antibody, and then Kar3-Cik1 motors were introduced into the flow chamber, along with Alexa 647-labeled cargo microtubules. Using this assay, motor-associated alignment and sliding of microtubules were observed: Kar3-Cik1 motors acted to pivot the blue (Alexa 647) cargo microtubule into alignment with the red (rhodamine) coverslip-attached microtubule and then subsequently to slide the blue cargo microtubule along the red microtubule (Figures 4D and S4; Movies S4, S5, S6, and S7). These pivoting and sliding events were observed both in the presence and in the absence of the GST tag on Cik1 (Figure S4), and observations of motor directionality on aligned microtubules indicated that the Kar3-Cik1 motors aligned both parallel and antiparallel microtubules, consistent with simulation assumptions (Movies S4, S5, S6, and S7).

As a further test of Kar3-Cik1 crosslinking activity, red and green stabilized microtubules were incubated together in tubes both with and without Kar3-Cik1, and the mixtures were then visualized on coverslips using TIRF microscopy. While there was no crosslinking of the red and green microtubules from

(B) All observations demonstrated minus-end-directed Kar3/Cik1 motility.
(C) Negative-stained TEM images provide evidence for single-molecule microtubule binding events (yellow circles). The red and green arrows (right) are suggestive of Kar3-Cik1 motor-heads (inset scale bars, 25 nm).
(D) In vitro Kar3-Cik1 motors (green) act to pivot and slide the cargo Alexa 647 microtubules (blue) relative to the coverslip-attached rhodamine microtubules (red) (Movies S4, S5, S6, and S7) (scale bar, 2 μm).
(E) Kar3-Cik1 robustly crosslinks red and green microtubules in a bulk bundling experiment.

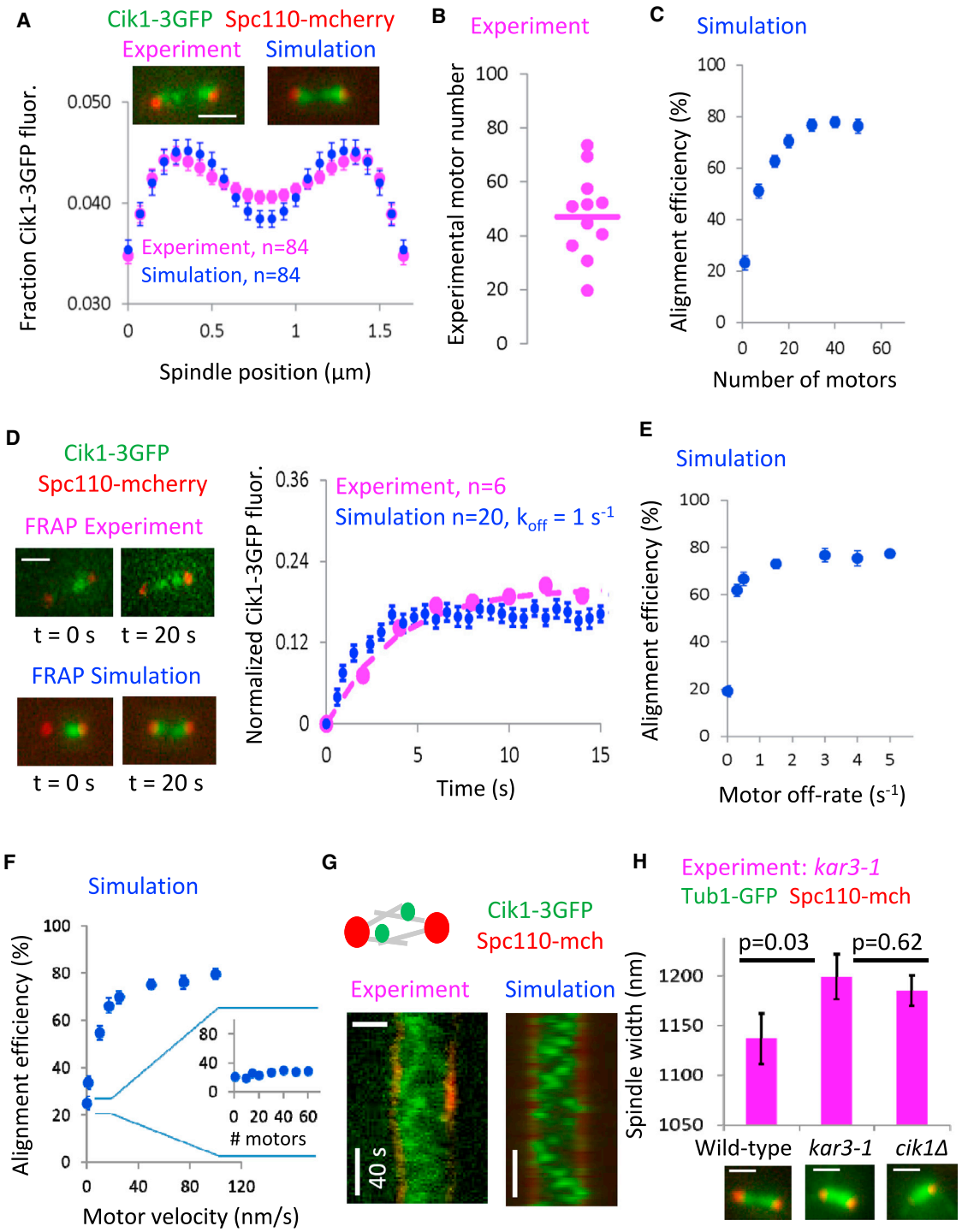

Figure 5. The Localization and Dynamics of Kar3/Cik1 Are Consistent with Simulation Predictions for Its Role in Midzone Microtubule Alignment

(A) Simulations predict (blue) and experiments confirm (magenta) that Kar3-Cik1 is localized just outside of the midzone, near to the spindle poles ($p = 0.79$, K-S test) (scale bar, 1,000 nm).

(B and C) Experimentally estimated motor numbers (B; see Supplemental Experimental Procedures) are consistent with (C) simulations that predict that ≥20 Kar3-Cik1 motors numbers could result in reasonable midzone microtubule alignment efficiency.

(D and E) Experimental and simulated FRAP experiments. A reasonable fit between experiments and simulations is achieved using $k_{off} = 1\ s^{-1}$ for Kar3-Cik1 motor interaction with microtubules (D), which is (E) an off-rate that simulations predict should produce efficient midzone microtubule alignment.

(legend continued on next page)

the control tube (Figure 4E, left), after a 30 min incubation with Kar3-Cik1, 67% of the microtubules were in large bundles of red and green microtubules (Figure 4E, right). Thus, in vitro experiments provide evidence that Kar3-Cik1 crosslinking may act to align and bundle microtubules in the mitotic spindle. Simulations and experiments were then used to directly test model predictions.

In Vivo Kar3-Cik1 Localization Is Consistent with Simulation Predictions for Its Role in Spindle Microtubule Alignment

We first evaluated the localization of Cik1-3xGFP in the yeast metaphase spindle. Here, simulations predict, and TIRF microscopy experiments confirm, that while functional experiments demonstrate that Kar3-Cik1 acts to maintain the structure of the spindle midzone, Cik1-3xGFP is most strongly concentrated just outside of the spindle midzone (Figure 5A; p = 0.79, Kolmogorov-Smirnov [K-S] test). This result provides an interesting example in which the localization of a protein does not coincide with its function: Kar3-Cik1 has an important role in establishing a functional mitotic spindle midzone, even though it is predominantly localized outside of the midzone.

In Vivo Kar3-Cik1 Molecule Numbers Are Consistent with Simulation Predictions for Efficient Spindle Microtubule Alignment

Next, we asked whether the number of Kar3-Cik1 motors present inside of cells is predicted to be sufficient to perform the spindle microtubule alignment function. The average number of experimental Kar3-Cik1 motors attached to the spindle was estimated using counting statistics (Rosenfeld et al., 2006; Teng et al., 2010) (see Supplemental Experimental Procedures), and we found that there were, on average, ~47 Kar3-Cik1 motors attached to the experimental spindles at any given time (Figure 5B). Then, by performing simulations that included different numbers of motors, it was determined that, similar to our experimental estimates, 30–50 simulated minus-end-directed motors were sufficient to efficiently align midzone microtubules during the 15 min simulation duration (Figure 5C). This is a timescale that is similar to metaphase duration in yeast ((Pearson et al., 2001), although many spindles were well aligned on a much shorter timescale (e.g., see Movie S2; $t_{duration}$ = 123 s).

Rapid In Vivo Kar3-Cik1 Unbinding Kinetics Is Consistent with Simulation Predictions for Efficient Spindle Microtubule Alignment

To characterize the relationship between Kar3-Cik1 spindle unbinding kinetics and the efficiency of spindle microtubule alignment, Kar3-Cik1 turnover on the spindle was evaluated using fluorescence recovery after photobleaching (FRAP) experiments. Here, the Cik1-3xGFP fluorescence in half of the metaphase spindle was photobleached, and then fluorescence recovery was observed (Figure 5D, left top). By fitting to an exponential recovery, the FRAP half-time was experimentally determined to be $t_{1/2} \sim 2.6$ s (Figure 5D, right, magenta). This value was then used to constrain the simulated Kar3-Cik1 off-rate constant (k_{off}) by performing simulated FRAP experiments (Figure 5D, left bottom). We found a reasonable fit between experiment and simulation using $k_{off} = 1\ s^{-1}$ (Figure 5D, right, blue). This in vivo value for k_{off} is higher than was observed for the highly processive in vitro Kar3-Cik1 motors, perhaps due to the high concentration of short (~300 nm), highly dynamic microtubules in the yeast metaphase spindle.

Simulation predictions were then made regarding the effect of motor off-rate (k_{off}) on midzone microtubule alignment efficiency. Here, the simulated midzone microtubule alignment efficiency was measured as a function of k_{off}, for v_{motor} = 50 nm/s and N_{motor} = 30 motors. While the alignment efficiency appeared to drop off rapidly for $k_{off} < 0.3\ s^{-1}$, the simulated midzone alignment efficiency was relatively robust for $k_{off} \geq 0.3\ s^{-1}$ (Figure 5E). We speculate that because the Kar3-Cik1 motor concentration is relatively low, rapid motor turnover on the spindle may release motors from "unproductive" attachments and thus allow the motors to rapidly search out and correct splayed interpolar microtubules.

Efficient Midzone Alignment Requires Kar3-Cik1 Motility, Both Experimentally and in Simulation

Finally, the importance of Kar3-Cik1 motility was evaluated by measuring the sensitivity of spindle microtubule alignment efficiency to a range of motor velocity values, with $k_{off} = 1\ s^{-1}$. The most important prediction here was that motor motility was required for efficient microtubule alignment: similar to the diffusion-only simulations (Figure 3D), simulations with stationary motors (i.e., v_{motor} = 0 nm/s) resulted in a poor efficiency of microtubule alignment (~20%), even though the motors were allowed to passively crosslink the spindle microtubules (Figure 5F), regardless of the number of stationary motors included in the simulation (Figure 5F, inset). However, the alignment efficiency was relatively constant for $v_{motor} \geq 30$ nm/s (Figure 5F).

In experiments, Cik1-3GFP motility was clearly observed in spindle kymographs (Figure 5G, left). Similarly, even though the simulation off-rate was assigned as $k_{off} = 1\ s^{-1}$, motility was also observed in artificial kymographs generated by the simulation (Figure 5G, right). Therefore, while the in vivo run length of individual Kar3-Cik1 motors is likely to be short, the collective movements of multiple molecules can be observed streaming toward the minus ends of the spindle microtubules.

To ask whether a reduced motor velocity would experimentally reduce the spindle microtubule alignment, we used a previously described *kar3-1* mutant that results in rigor binding of the motor-head to the microtubule (Meluh and Rose, 1990). Importantly, *kar3-1* mutant spindles trended toward the *cik1Δ* phenotype: spindle lengths were quantitatively shorter and wider than in WT spindles (Figure 5H; WT spindle length = 1,353 ± 18 nm [mean ± SEM]; *kar3-1* spindle length = 1,177 ± 32 nm,

(F) Simulations predict that minus-end-directed motility is critical for midzone microtubule alignment (inset shows results for increasing numbers of stationary motors).
(G) Motility of spindle-associated Kar3-Cik1 motors (scale bar, 500 nm) in experiments (left) and simulations (right).
(H) Consistent with simulation predictions, a *kar3-1* motor rigor mutant shows wider spindle morphology, similar to *cik1Δ* spindles (WT, n = 392; *kar3-1*, n = 199; *cik1Δ*, n = 219; error bars show SEM).

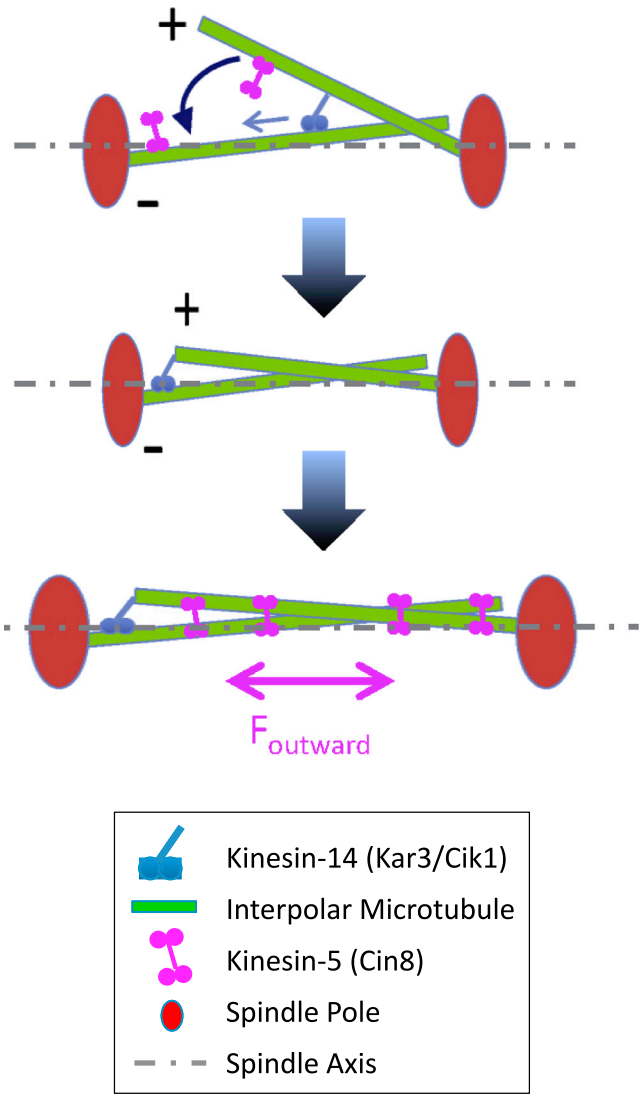

Figure 6. Model for How Minus-End-Directed Kinesin-14 Motors Could Align Antiparallel Microtubules to Extend Metaphase Spindle Lengths

In this model, as the Kar3-Cik1 minus-end-directed motor-head (blue circles) moves toward the spindle poles, the tail travels with the head (blue line), remaining attached to its crosslinked microtubule. This action results in "zippering" of the splayed microtubule (green) toward the spindle axis as the minus-end-directed motor-head walks toward the spindle pole to which its microtubule is attached. This action leads to a functional midzone, with spindle microtubules tightly aligned parallel to the spindle axis. Thus, minus-end-directed kinesin-14 molecular motors then allow for proper targeting and crosslinking of kinesin-5 molecular motors (magenta) in the spindle midzone, leading to an increase in outwardly directed spindle forces, and longer spindles.

$p << 0.0001$; spindle width, $p = 0.03$), suggesting that midzone microtubules were not properly aligned. In addition, the mean spindle widths were statistically indistinguishable between *cik1Δ* and *kar3-1* spindles (Figure 5H; $p = 0.62$). We conclude that the Kar3-Cik1 molecular motors are motile in the metaphase mitotic spindle and that this motility is required for efficient alignment of spindle microtubules during metaphase.

DISCUSSION

In conclusion, we propose that minus-end-directed kinesin-14 motors align antiparallel microtubules along the spindle axis during metaphase (Figure 6, top) and thus allow kinesin-5 motors to generate outwardly directed spindle forces (Figure 6, bottom). This mechanism can explain why kinesin-14 inactivation leads to shorter, unstable metaphase spindle lengths across a number of different cell types (Table 1). While any crosslinking protein may act to bundle microtubules, minus-end-directed Kar3-Cik1 kinesin-14 motors have the important ability to spatially align microtubules along the spindle axis. This is because the spindle microtubule minus ends are anchored at the poles, and so the minus-end-directed Kar3-Cik1 motors act to pivot splayed microtubules from the opposite pole into alignment with the spindle pole bodies (Figure 6, top).

Previous reports assign passive crosslinking proteins such as Ase1 (PRC1 in humans) an important role in the bundling of midzone microtubules during anaphase (Braun et al., 2011; Janson et al., 2007; Kapitein et al., 2005; Kotwaliwale et al., 2007; Loïodice et al., 2005; Schuyler et al., 2003). Similar to our simulation assumptions, we expect that crosslinking proteins other than kinesin-14 may be required to maintain proper bundling within the midzone once interpolar microtubules are pivoted into alignment with the central spindle axis. Therefore, additional crosslinking proteins may play a key role in maintaining proper midzone microtubule bundling during metaphase, while kinesin-14 molecular motors are able to actively pivot and thus spatially align spindle microtubules along the spindle axis.

We speculate that kinesin-14 molecular motors may serve a dual purpose in the force balance model for spindle length regulation: in addition to aligning spindle microtubules to build a functional midzone, thus allowing for an increase in outwardly directed forces, we speculate that kinesin-14 motors may also act at interpolar microtubule plus ends to directly generate inward forces, which could explain why overexpression of kinesin-14 motors leads to shorter mitotic spindles in yeast (Hildebrandt and Hoyt, 2000). In general, these results demonstrate that discerning a cellular-level function from a specific in vitro molecular function requires consideration of how each molecular species works in the context of other molecular species.

EXPERIMENTAL PROCEDURES

In Vitro Experiments

Purification of Kar3-Cik1 from yeast was based on the protocol described in Gerson-Gurwitz et al. (2011). In brief, strain YMG68, containing *CIK1*-GST and *KAR3*-GFP behind the *GAL1* promoter, was grown up, cells were harvested by centrifugation, and then frozen dropwise in liquid nitrogen. The cell lysate was centrifuged at 18,000 × *g*, 4°C, for 30 min, and the supernatant was saved. This soluble lysate was mixed with ~0.9 ml of glutathione Sepharose 4B beads (GE Healthcare). The proteins were eluted by mixing the beads four times for 10 min at 4°C in 0.5 ml of MB175 buffer + 1× protease inhibitors, 1% Triton X-100, and10 mM reduced glutathione. Solutions were collected after each elution, snap frozen, and stored in liquid nitrogen. Stabilized microtubule seeds were made and imaging chambers constructed as previously described (Gell et al., 2010), with details in Supplemental Experimental Procedures.

Motor Protein Motility Assays

Following addition of microtubules, the chamber was incubated for ~5 min, and the chamber was washed of nonbound microtubules by flowing through

of 100 μl of 80 mM PIPES buffer (pH 6.8) containing 1 mM EGTA and 1 mM $MgCl_2$ (Brb80). Then, 100 μl of imaging buffer was added to the chamber, consisting of 20 mM D-glucose, 90 μg/ml casein, 10 μg/ml catalase, 20 μg/ml glucose oxidase, 10 mM dithiothreitol, 2 mM ATP, 1% Tween 20, and 75 mM KCl (except as specified otherwise for Figure S5) in Brb80. Lastly, 50 μl of reaction mixture identical to the imaging buffer, except for the addition of motor protein, was added to the chamber.

The gliding assay was identical to the motility assay, except that after Kar3-Cik1 motors were introduced to the chamber and allowed to adhere to the microtubules, the chamber was then flushed with the identical Kar3-Cik1 motor reaction mixture again, and cargo microtubules were included in the new mixture (Alexa 647-labeled GMPCPP microtubules).

To perform the bulk crosslinking assay, green Alexa 488- and red rhodamine-labeled seeds were premade, spun down, and resuspended in Brb80. Then, red and green seeds were mixed together with either Brb80, or with Kar3-Cik1 and a correspondingly lower amount of Brb80, so that total volumes in each case were identical. Both control and experimental mixtures were then incubated for 30 or 60 min at 30°C in a dark room. Finally, 5 μl of the control or experimental mixtures was placed on a slide, a coverslip was placed on top of the drop, and the edges were sealed with clear nail polish. Images were then taken in TIRF as described above. Percent of bundling was quantified by counting the number of bundled and unbundled microtubules on each image.

TEM

To visualize Kar3-Cik1 protein bound to microtubules using TEM, GMPCPP seeds were added to motor buffer and purified Kar3-Cik1 protein. A drop of the seed, protein, and motor buffer mixture was placed on a 300-mesh carbon-coated copper grid for 1 min. At 1 min, the grid was washed with six drops of motor buffer and then stained with 1% uranyl acetate for 1 min. The stain was then wicked away with filter paper, and the grid was left to dry and then stored. Specimens were observed using an FEI Technai Spirit BioTWIN transmission electron microscope. Images were recorded at 15,000–20,000× at −3 to −5 defocus.

Electron Tomography

Cells were prepared for electron tomography using methods published previously (Giddings et al., 2001) and described in Supplemental Experimental Procedures.

In Vivo Yeast Mitotic Spindle Imaging

All yeast strains were grown overnight and then immobilized during imaging on a coverslip to allow for TIRF imaging. Flow chambers for imaging live yeast cells were constructed, and image analysis was performed per detailed descriptions in Supplemental Experimental Procedures.

Statistical Analysis

All reported t tests were two-tailed t tests, assuming two samples with unequal variance. A two-sample K-S test was used to compare simulation to experiment using the MATLAB function *kstest2* with option significance level 0.01.

SUPPLEMENTAL INFORMATION

Supplemental Information includes Supplemental Experimental Procedures, four figures, and seven movies and can be found with this article online at http://dx.doi.org/10.1016/j.devcel.2014.07.023.

AUTHOR CONTRIBUTIONS

A.J.H. wrote and executed simulations. P.T.W. performed in vitro and in vivo experiments.

ACKNOWLEDGMENTS

M.K.G. is supported by the Pew Charitable Trusts through the Pew Scholars Program in the Biomedical Sciences and by NIH grant NIGMS GM-103833. The Boulder Laboratory for 3D EM of Cells is supported by grant P41GM103431-42 from NIGMS to Andreas Hoenger. D.J.O. is supported by NIH grant GM-071522. Parts of this work were carried out in the Characterization Facility, University of Minnesota, a member of the NSF-funded Materials Research Facilities Network (http://www.mrfn.org) via the MRSEC program.

Received: October 31, 2013
Revised: May 28, 2014
Accepted: July 29, 2014
Published: October 13, 2014

REFERENCES

Allingham, J.S., Sproul, L.R., Rayment, I., and Gilbert, S.P. (2007). Vik1 modulates microtubule-Kar3 interactions through a motor domain that lacks an active site. Cell *128*, 1161–1172.

Ambrose, J.C., and Cyr, R. (2007). The kinesin ATK5 functions in early spindle assembly in Arabidopsis. Plant Cell *19*, 226–236.

Barrett, J.G., Manning, B.D., and Snyder, M. (2000). The Kar3p kinesin-related protein forms a novel heterodimeric structure with its associated protein Cik1p. Mol. Biol. Cell *11*, 2373–2385.

Braun, M., Lansky, Z., Fink, G., Ruhnow, F., Diez, S., and Janson, M.E. (2011). Adaptive braking by Ase1 prevents overlapping microtubules from sliding completely apart. Nat. Cell Biol. *13*, 1259–1264.

Cai, S., Weaver, L.N., Ems-McClung, S.C., and Walczak, C.E. (2009). Kinesin-14 family proteins HSET/XCTK2 control spindle length by cross-linking and sliding microtubules. Mol. Biol. Cell *20*, 1348–1359.

Cottingham, F.R., Gheber, L., Miller, D.L., and Hoyt, M.A. (1999). Novel roles for *saccharomyces cerevisiae* mitotic spindle motors. J. Cell Biol. *147*, 335–350.

Endow, S.A., Kang, S.J., Satterwhite, L.L., Rose, M.D., Skeen, V.P., and Salmon, E.D. (1994). Yeast Kar3 is a minus-end microtubule motor protein that destabilizes microtubules preferentially at the minus ends. EMBO J. *13*, 2708–2713.

Enos, A.P., and Morris, N.R. (1990). Mutation of a gene that encodes a kinesin-like protein blocks nuclear division in A. nidulans. Cell *60*, 1019–1027.

Furuta, K., and Toyoshima, Y.Y. (2008). Minus-end-directed motor Ncd exhibits processive movement that is enhanced by microtubule bundling in vitro. Curr. Biol. *18*, 152–157.

Gardner, M.K., Pearson, C.G., Sprague, B.L., Zarzar, T.R., Bloom, K., Salmon, E.D., and Odde, D.J. (2005). Tension-dependent regulation of microtubule dynamics at kinetochores can explain metaphase congression in yeast. Mol. Biol. Cell *16*, 3764–3775.

Gardner, M.K., Bouck, D.C., Paliulis, L.V., Meehl, J.B., O'Toole, E.T., Haase, J., Soubry, A., Joglekar, A.P., Winey, M., Salmon, E.D., et al. (2008a). Chromosome congression by Kinesin-5 motor-mediated disassembly of longer kinetochore microtubules. Cell *135*, 894–906.

Gardner, M.K., Haase, J., Mythreye, K., Molk, J.N., Anderson, M., Joglekar, A.P., O'Toole, E.T., Winey, M., Salmon, E.D., Odde, D.J., and Bloom, K. (2008b). The microtubule-based motor Kar3 and plus end-binding protein Bim1 provide structural support for the anaphase spindle. J. Cell Biol. *180*, 91–100.

Gell, C., Bormuth, V., Brouhard, G.J., Cohen, D.N., Diez, S., Friel, C.T., Helenius, J., Nitzsche, B., Petzold, H., Ribbe, J., et al. (2010). Microtubule dynamics reconstituted in vitro and imaged by single-molecule fluorescence microscopy. Methods Cell Biol. *95*, 221–245.

Gerson-Gurwitz, A., Thiede, C., Movshovich, N., Fridman, V., Podolskaya, M., Danieli, T., Lakämper, S., Klopfenstein, D.R., Schmidt, C.F., and Gheber, L. (2011). Directionality of individual kinesin-5 Cin8 motors is modulated by loop 8, ionic strength and microtubule geometry. EMBO J. *30*, 4942–4954.

Ghosh, S., Hentrich, C., and Surrey, T. (2013). Micropattern-controlled local microtubule nucleation, transport, and mesoscale organization. ACS Chem. Biol. *8*, 673–678.

Giddings, T.H., Jr., O'Toole, E.T., Morphew, M., Mastronarde, D.N., McIntosh, J.R., and Winey, M. (2001). Using rapid freeze and freeze-substitution for the preparation of yeast cells for electron microscopy and three-dimensional analysis. Methods Cell Biol. *67*, 27–42.

Goshima, G., and Scholey, J.M. (2010). Control of mitotic spindle length. Annu. Rev. Cell Dev. Biol. *26*, 21–57.

Goshima, G., Nédélec, F., and Vale, R.D. (2005). Mechanisms for focusing mitotic spindle poles by minus end-directed motor proteins. J. Cell Biol. *171*, 229–240.

Hildebrandt, E.R., and Hoyt, M.A. (2000). Mitotic motors in Saccharomyces cerevisiae. Biochim. Biophys. Acta *1496*, 99–116.

Huyett, A., Kahana, J., Silver, P., Zeng, X., and Saunders, W.S. (1998). The Kar3p and Kip2p motors function antagonistically at the spindle poles to influence cytoplasmic microtubule numbers. J. Cell Sci. *111*, 295–301.

Janson, M.E., Loughlin, R., Loïodice, I., Fu, C., Brunner, D., Nédélec, F.J., and Tran, P.T. (2007). Crosslinkers and motors organize dynamic microtubules to form stable bipolar arrays in fission yeast. Cell *128*, 357–368.

Kalinina, I., Nandi, A., Delivani, P., Chacón, M.R., Klemm, A.H., Ramunno-Johnson, D., Krull, A., Lindner, B., Pavin, N., and Tolić-Nørrelykke, I.M. (2013). Pivoting of microtubules around the spindle pole accelerates kinetochore capture. Nat. Cell Biol. *15*, 82–87.

Kapitein, L.C., Peterman, E.J., Kwok, B.H., Kim, J.H., Kapoor, T.M., and Schmidt, C.F. (2005). The bipolar mitotic kinesin Eg5 moves on both microtubules that it crosslinks. Nature *435*, 114–118.

Kashina, A.S., Baskin, R.J., Cole, D.G., Wedaman, K.P., Saxton, W.M., and Scholey, J.M. (1996). A bipolar kinesin. Nature *379*, 270–272.

Kotwaliwale, C.V., Frei, S.B., Stern, B.M., and Biggins, S. (2007). A pathway containing the Ipl1/aurora protein kinase and the spindle midzone protein Ase1 regulates yeast spindle assembly. Dev. Cell *13*, 433–445.

Kwon, M., Godinho, S.A., Chandhok, N.S., Ganem, N.J., Azioune, A., Thery, M., and Pellman, D. (2008). Mechanisms to suppress multipolar divisions in cancer cells with extra centrosomes. Genes Dev. *22*, 2189–2203.

Loïodice, I., Staub, J., Setty, T.G., Nguyen, N.P., Paoletti, A., and Tran, P.T. (2005). Ase1p organizes antiparallel microtubule arrays during interphase and mitosis in fission yeast. Mol. Biol. Cell *16*, 1756–1768.

Manning, B.D., Barrett, J.G., Wallace, J.A., Granok, H., and Snyder, M. (1999). Differential regulation of the Kar3p kinesin-related protein by two associated proteins, Cik1p and Vik1p. J. Cell Biol. *144*, 1219–1233.

Meluh, P.B., and Rose, M.D. (1990). KAR3, a kinesin-related gene required for yeast nuclear fusion. Cell *60*, 1029–1041.

Middleton, K., and Carbon, J. (1994). KAR3-encoded kinesin is a minus-end-directed motor that functions with centromere binding proteins (CBF3) on an in vitro yeast kinetochore. Proc. Natl. Acad. Sci. USA *91*, 7212–7216.

O'Toole, E.T., Winey, M., and McIntosh, J.R. (1999). High-voltage electron tomography of spindle pole bodies and early mitotic spindles in the yeast Saccharomyces cerevisiae. Mol. Biol. Cell *10*, 2017–2031.

Page, B.D., and Snyder, M. (1992). CIK1: a developmentally regulated spindle pole body-associated protein important for microtubule functions in Saccharomyces cerevisiae. Genes Dev. *6*, 1414–1429.

Page, B.D., Satterwhite, L.L., Rose, M.D., and Snyder, M. (1994). Localization of the Kar3 kinesin heavy chain-related protein requires the Cik1 interacting protein. J. Cell Biol. *124*, 507–519.

Pearson, C.G., Maddox, P.S., Salmon, E.D., and Bloom, K. (2001). Budding yeast chromosome structure and dynamics during mitosis. J. Cell Biol. *152*, 1255–1266.

Portran, D., Gaillard, J., Vantard, M., and Thery, M. (2013). Quantification of MAP and molecular motor activities on geometrically controlled microtubule networks. Cytoskeleton (Hoboken) *70*, 12–23.

Roof, D.M., Meluh, P.B., and Rose, M.D. (1991). Multiple kinesin-related proteins in yeast mitosis. Cold Spring Harb. Symp. Quant. Biol. *56*, 693.

Roof, D.M., Meluh, P.B., and Rose, M.D. (1992). Kinesin-related proteins required for assembly of the mitotic spindle. J. Cell Biol. *118*, 95–108.

Rosenfeld, N., Perkins, T.J., Alon, U., Elowitz, M.B., and Swain, P.S. (2006). A fluctuation method to quantify in vivo fluorescence data. Biophys. J. *91*, 759–766.

Saunders, W.S., and Hoyt, M.A. (1992). Kinesin-related proteins required for structural integrity of the mitotic spindle. Cell *70*, 451–458.

Saunders, W., Hornack, D., Lengyel, V., and Deng, C. (1997a). The Saccharomyces cerevisiae kinesin-related motor Kar3p acts at preanaphase spindle poles to limit the number and length of cytoplasmic microtubules. J. Cell Biol. *137*, 417–431.

Saunders, W., Lengyel, V., and Hoyt, M.A. (1997b). Mitotic spindle function in Saccharomyces cerevisiae requires a balance between different types of kinesin-related motors. Mol. Biol. Cell *8*, 1025–1033.

Sawin, K.E., LeGuellec, K., Philippe, M., and Mitchison, T.J. (1992). Mitotic spindle organization by a plus-end-directed microtubule motor. Nature *359*, 540–543.

Schuyler, S.C., Liu, J.Y., and Pellman, D. (2003). The molecular function of Ase1p: evidence for a MAP-dependent midzone-specific spindle matrix. Microtubule-associated proteins. J. Cell Biol. *160*, 517–528.

Sharp, D.J., Brown, H.M., Kwon, M., Rogers, G.C., Holland, G., and Scholey, J.M. (2000). Functional coordination of three mitotic motors in Drosophila embryos. Mol. Biol. Cell *11*, 241–253.

Sherwood, R.K., and Bennett, R.J. (2008). Microtubule motor protein Kar3 is required for normal mitotic division and morphogenesis in Candida albicans. Eukaryot. Cell *7*, 1460–1474.

Shimizu, T., Toyoshima, Y.Y., Edamatsu, M., and Vale, R.D. (1995). Comparison of the motile and enzymatic properties of two microtubule minus-end-directed motors, ncd and cytoplasmic dynein. Biochemistry *34*, 1575–1582.

Subramanian, R., and Kapoor, T.M. (2012). Building complexity: insights into self-organized assembly of microtubule-based architectures. Dev. Cell *23*, 874–885.

Teng, S.W., Wang, Y., Tu, K.C., Long, T., Mehta, P., Wingreen, N.S., Bassler, B.L., and Ong, N.P. (2010). Measurement of the copy number of the master quorum-sensing regulator of a bacterial cell. Biophys. J. *98*, 2024–2031.

Troxell, C.L., Sweezy, M.A., West, R.R., Reed, K.D., Carson, B.D., Pidoux, A.L., Cande, W.Z., and McIntosh, J.R. (2001). pkl1(+)and klp2(+): Two kinesins of the Kar3 subfamily in fission yeast perform different functions in both mitosis and meiosis. Mol. Biol. Cell *12*, 3476–3488.

Varga, V., Helenius, J., Tanaka, K., Hyman, A.A., Tanaka, T.U., and Howard, J. (2006). Yeast kinesin-8 depolymerizes microtubules in a length-dependent manner. Nat. Cell Biol. *8*, 957–962.

Walczak, C.E., Vernos, I., Mitchison, T.J., Karsenti, E., and Heald, R. (1998). A model for the proposed roles of different microtubule-based motor proteins in establishing spindle bipolarity. Curr. Biol. *8*, 903–913.

Winey, M., Mamay, C.L., O'Toole, E.T., Mastronarde, D.N., Giddings, T.H., Jr., McDonald, K.L., and McIntosh, J.R. (1995). Three-dimensional ultrastructural analysis of the Saccharomyces cerevisiae mitotic spindle. J. Cell Biol. *129*, 1601–1615.

Yuen, K.W., Warren, C.D., Chen, O., Kwok, T., Hieter, P., and Spencer, F.A. (2007). Systematic genome instability screens in yeast and their potential relevance to cancer. Proc. Natl. Acad. Sci. USA *104*, 3925–3930.